Lifetimes of yrast and near-yrast states of ^{159,160,161}Yb

M. P. Fewell,* N. R. Johnson, F. K. McGowan, J. S. Hattula,†
I. Y. Lee, C. Baktash, and Y. Schutz‡
Oak Ridge National Laboratory, Oak Ridge, Tennessee 37831

J. C. Wells
Tennessee Technological University, Cookeville, Tennessee 38505
and Oak Ridge National Laboratory, Oak Ridge, Tennessee 37831

L. L. Riedinger and M. W. Guidry
University of Tennessee, Knoxville, Tennessee 37996
and Oak Ridge National Laboratory, Oak Ridge, Tennessee 37831

S. C. Pancholi
University of Delhi, Delhi 110007, India
and Vanderbilt University, Nashville, Tennessee 37325

(Received 20 July 1987)

Lifetimes of high-spin states of ^{159,160,161}Yb, populated by fusion-evaporation reactions, have been measured by the recoil-distance technique. The data were collected in coincidence with a total-energy filter to provide some discrimination on reaction channel. The principal feature of the resulting transition quadrupole moments is a frequency-dependent reduction which is displayed by those bands with aligned quasiparticles. This seems to be mainly due to the influence of the favored $i_{13/2}$ quasineutron. Additional available data are surveyed and support this conclusion. Calculations using the cranked shell model and the cranked Hartree-Fock-Bogoliubov and cranked Nilsson-Strutinsky methods provide a qualitative description of the experimental observations. In addition, a satisfactory account is provided by recent calculations based on a fermion dynamical-symmetry model.

I. INTRODUCTION

The spectroscopy of the yrast and near-yrast bands of the $N=88-98$ isotones of rare-earth nuclei has been an area of intense interest in recent years. Most of the high-spin data can be understood, at least qualitatively, in terms of aligned high-j nucleons weakly coupled to deformed cores with rather constant deformation parameters (the cranked shell model[1]). However, the neglect of variations in deformation from state to state is dangerous in the $N=88-90$ transition region between rotational and vibrational nuclei. It has been known for some time that the ground-state bands of the even-even $N=90$ nuclei [for example, ^{150}Nd (Ref. 2)] exhibit centrifugal stretching; that is, the collectivity increases with increasing angular momentum. On the other hand, recent lifetime measurements on ^{156,158}Dy (Refs. 3 and 4) and ^{158}Er (Ref. 5) indicate that the collectivity of the s bands of these nuclei is reduced relative to that of their respective ground-state bands. It is the relationship between these changes in collectivity and the alignment of various high-j quasiparticles that this work addresses through the measurement of lifetimes of high-spin states.

The nuclei ^{159,160,161}Yb provide excellent opportunities to test the quasiparticle dependence of collectivity because, in previous extensive spectroscopic investigations,[6-10] it has been observed that there are distinct band crossings leading to bands with rather large aligned angular momenta. These band crossings, which are due to the alignment of both quasineutrinos and quasiprotons, are generally sharp in this region. This makes it possible to associate measured transition probabilities with the degree of collectivity of the aligned bands, many of which have been identified with a variety of multiquasiparticle configurations. Lifetimes are reported here for states in a number of these bands. In ^{160}Yb we have measured lifetimes in the ground band and three aligned two-quasiparticle bands: AB (the yrast band after the first backbend), AE, and AF, where, as usual, A and B refer to the two lowest-energy $i_{13/2}$ quasineutron excitations and E and F to the lowest negative-parity states (mostly $h_{9/2}$ in origin). Lifetimes are also reported here for states in the $vi_{13/2}$ band A of ^{159}Yb and in the one-quasiparticle bands A and E and three-quasiparticle band EAB of ^{161}Yb. Preliminary reports of this work have previously appeared.[11-14]

Sections II and III describe the experiment and its analysis. Results are presented in Sec. IV. A comparison of the results for ^{160}Yb and ^{161}Yb reveals several of the effects of quasiparticle alignment on collectivity. This is discussed in Sec. V A and the present results are related to some of the systematics of the $N=89-91$ nuclei in Sec. V B. In Sec. V C the results are considered in light of recent theoretical calculations. In particular, Bengtsson *et al.*[15] and Tanabe *et al.*[16] performed self-consistent calculations of the shape parameters for the

ground and s bands of ^{160}Yb, on the basis of which they suggest that the $i_{13/2}$ quasineutrons drive the nucleus to increasingly triaxial shapes as the angular momentum is increased. This is qualitatively in agreement with the present findings, as are the calculations of Chen *et al.*,[17] who have used a phenomenological cranked-shell-model approach to associate the observed decrease of collectivity in ^{160}Yb with the alignment of both $i_{13/2}$ and $h_{9/2}$ quasineutrons. In addition, satisfactory agreement is obtained from recent calculations using a fermion dynamical-symmetry model.[18] The conclusions are summarized in Sec. VI.

II. EXPERIMENTAL METHOD

High-spin states of nuclei in the region of ^{160}Yb were produced by fusion-evaporation reactions with heavy ions. Two experiments were performed: a "normal kinematics reaction" with a 205-MeV ^{48}Ti beam from the 25-MV tandem accelerator at Oak Ridge National Laboratory incident on a ^{116}Cd target and an "inverse kinematics reaction" with a 495-MeV ^{116}Cd beam and a ^{48}Ti target. The second beam, which provided a much larger recoil velocity, was obtained by injecting a 111-MeV ^{116}Cd beam from the tandem accelerator into the Oak Ridge Isochronous Cyclotron (ORIC).

The recoil-distance device used in these measurements was designed so that the target could be located at the center of a large annular annular sodium-iodide (NaI) detector. Details of this device can be found in Refs. 19 and 20. The NaI detector was operated as a total γ-ray–energy summing device to provide some discrimination between reaction channels. The usefulness of total-energy filtering in these measurements can be assessed from Fig. 1, which presents data obtained with the ^{48}Ti-induced reaction in ^{116}Cd. It shows spectra from the NaI summing detector in coincidence with various γ rays detected by the Ge(Li) detector. The origins of these γ rays have been identified in previous spectroscopic work. In order from the top, Fig. 1 shows total-energy spectra from (a) all nuclei produced, (b) ^{116}Cd (inelastic scattering), (c) ^{159}Yb, (d) ^{157}Er, (e) ^{160}Yb, and (f) ^{161}Yb. Although the shape of the total-energy spectrum, in principle, depends on the position of the coincident γ ray in the yrast sequence, this dependence is much less than that due to reaction channel and was not noticeable in the present experiments. It is clear from Fig. 1 that one cannot obtain complete separation of the reaction channels, but that some selectivity is possible. The final choice of total-energy gates involves a compromise between selectivity and statistics.

For the ^{48}Ti-induced reaction, a 1.5-mg/cm^2-thick metallic target enriched to 98% in ^{116}Cd was used. The stopper consisted of a 1.27-μm-thick nickel foil which was stretched before coating with 30 mg/cm^2 of lead. The beam energy of 205 MeV was chosen to maximize the yield of the 4n reaction leading to ^{160}Yb. The recoil velocity of the ^{160}Yb nuclei, deduced from the energy separation of the shifted and unshifted peaks, was (6.877±0.024) μm/ps or $v/c=(2.294\pm0.008)\%$. Spectra were recorded at eleven target-stopper separations ranging from 25.3 μm to 2.02 mm. The position of zero separation was determined by the pulser-capacitance technique. In addition, the capacitance was monitored periodically during the course of the measurements. Illustrative spectra showing data from three target-stopper separations are presented in Fig. 2.

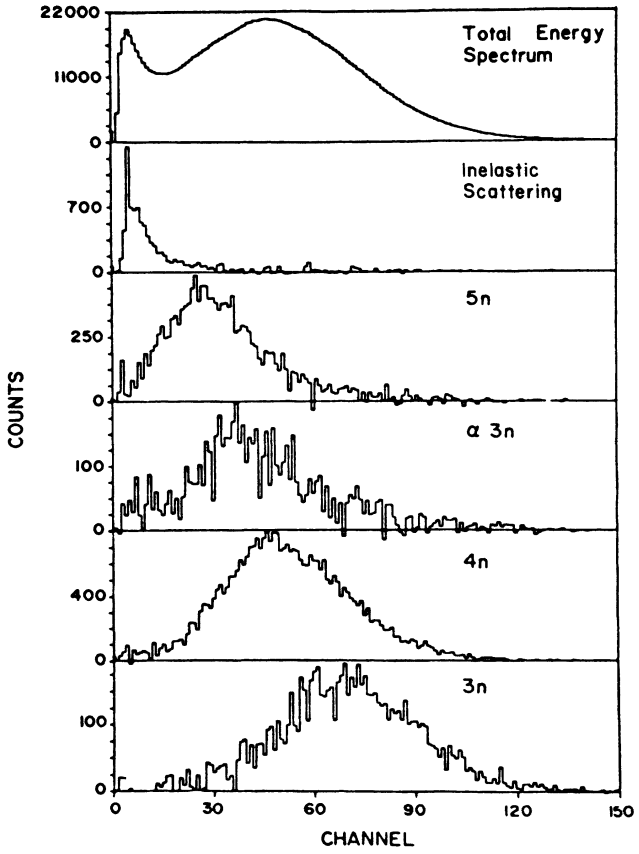

FIG. 1. Total-energy spectra resulting from 205-MeV ^{48}Ti bombardment of ^{116}Cd to produce the compound nucleus ^{164}Yb. The top spectrum is the spectrum of all prompt events in coincidence with the Ge counter, and the others result from gates on lines from the specified reactions. Full scale in energy is about 15 MeV.

The target for the ^{116}Cd-induced reaction was a 1.0-mg/cm^2-thick rolled metallic foil enriched to 99.1% in ^{48}Ti. The beam energy was chosen to give the same center-of-mass energy as in the reaction described above. The recoil velocity of the evaporation residues was sufficiently high that the stopping time in lead was comparable to the lifetimes of the states involved. Thus, had a lead stopper been used, many of the unshifted peaks would have been so Doppler broadened as to be indistinguishable from the background. Such a situation was observed[21] in a lifetime experiment on ^{156}Dy following the (^{136}Xe,4n) reaction. To avoid this difficulty, we elected to allow the recoils to pass through a 4.5-mg/cm^2 gold foil. Emling *et al.*[4] used a similar procedure. The recoils, together with the beam, were finally stopped in a thick lead foil placed about 10 mm behind the retarding foil. This distance was chosen so that only the ground

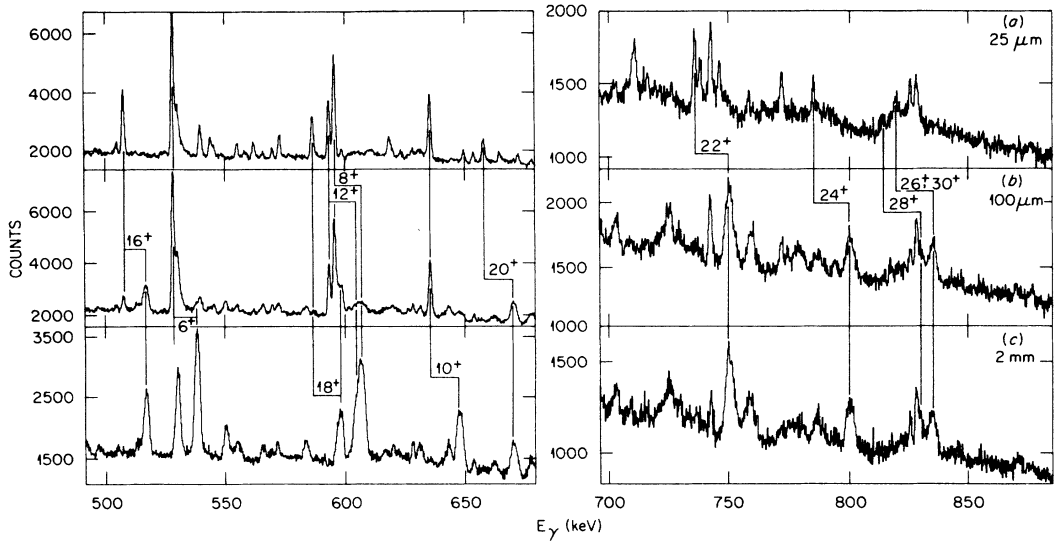

FIG. 2. Some γ-ray spectra in the "4n" gate from the ^{48}Ti-induced reaction. The target-stopper separations are (a) 25.3 μm, (b) 100.4 μm, and (c) 2.02 mm, with corresponding flight times of (a) 3.7 ps, (b) 14.6 ps, and (c) 294 ps. Only the members of the yrast sequence are labeled.

and first excited states had appreciable population by the time the recoils entered the lead stopper. Using the energy separation of the shifted, less shifted, and unshifted peaks from the $2^+ \rightarrow 0^+$ transition, we deduced that the recoil velocity was (19.34±0.15) μm/ps [$v/c = (6.45 \pm 0.05)\%$] before the retarding foil and 14 μm/ps afterwards.

With the ^{116}Cd-induced reaction, spectra were recorded at six target-retarder separations ranging from 176 μm to 2.65 mm. We were prevented from obtaining data at closer separations by the following difficulty with the target. During the experiment, a small dimple formed which projected upstream from the otherwise flat target surface. (We note that later tests with the same beam-target combination caused similar dimpling in similar target foils.) Examination of the decay curves showed them to be consistent with the dimple appearing relatively quickly during the initial focusing of the beam and remaining stable thereafter. That is, the decay curves obtained in this experiment could be matched with those obtained with the ^{48}Ti-induced reaction by a simple shift of origin, the shift required being 159±8 μm. (This was determined by least-squares fitting, as described in Sec. III C.) The degree of consistency achieved may be judged from the decay curves shown in Sec. IV A 1. Sample γ-ray spectra for this reaction are shown in Fig. 3.

III. DATA ANALYSIS

A. The extraction of the decay curves

The spectra, following gating with total energy, were fitted by standard techniques to obtained peak areas. Peak separations were calculated from the known γ-ray energies and the Doppler shifts were determined from the shifts of the most prominent peaks. The complexity of the spectra made it impossible to obtain the areas of both the shifted and unshifted (or less shifted) peaks of all transitions for every flight distance. Therefore, since it was not possible to normalize the intensities obtained at different flight distances with the sum of shifted and unshifted peaks, we have normalized with the intensity of the γ-ray continuum above about 950 keV, a pro-

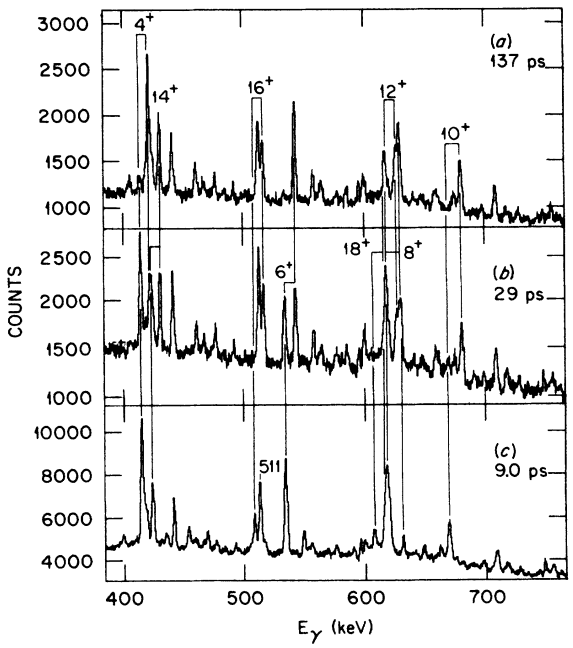

FIG. 3. Partial γ-ray spectra in the "4n" gate from the ^{116}Cd-induced reaction. Spectra for three different flight times are shown. Members of the yrast sequence are identified.

cedure which has previously been found[21] to be satisfactory.

A consequence of this method is that two decay curves are available for those transitions where the intensities of both the shifted and unshifted or less-shifted peaks could be extracted. As well as the familiar decay of the normalized unshifted intensity U (or, in the case of the experiment with the ^{116}Cd-induced reaction, the normalized less-shifted intensity L) with flight time, one also has the decay with flight time of the quantity I-S, where I is the total intensity of the γ ray and S is the normalized shifted intensity. These two decay curves are almost independent; the only correlation comes through I, which is determined by averaging the sums of the normalized intensities (i.e., $U+S$ or $L+S$ as the case may be) observed for each flight time. The values of $U+S$ or $L+S$ obtained for each flight distance are useful by-products of this method. If the data analysis, including the corrections described in the next section, is performed correctly, the $U+S$ and $L+S$ values should show no variation with flight distance.

The best resolution was obtained for the unshifted peaks observed with the ^{48}Ti-induced reaction. For example, the unshifted peaks corresponding to the $8^+\rightarrow 6^+$ and $12^+\rightarrow 10^+$ transitions were well resolved, whereas the corresponding shifted peaks were not (see Fig. 2). Spectra obtained with the ^{116}Cd-induced reaction had poorer resolution and higher backgrounds than those from the ^{48}Ti-induced reaction. However, because of the larger v/c, these spectra were useful in defining the decay curves for the ^{160}Yb yrast states with $I \leq 18$.

B. Corrections to the decay curves

In addition to the straightforward corrections for detection efficiency, coincidence efficiency, and internal conversion, there are four corrections which are usually applied to the normalized intensities obtained from recoil-distance experiments.[22] These are corrections for the apparent solid angle of the γ-ray detector, the attenuation of the angular distribution of the γ rays, the Doppler broadening of the unshifted or less-shifted peaks, and the time structure of the cascade feeding. When (heavy-ion,xn) reactions are used to populate the states of interest, this last correction is so significant as to dominate the analysis. Its treatment is discussed in Sec. III C. The solid-angle corrections are relatively minor. In the present experiment, their magnitudes were at most comparable with, and usually much smaller than, the uncertainties from spectrum analysis. The other two corrections are considered in the following subsections.

1. *The attenuation of the γ-ray angular distributions*

The correction for the vacuum depolarization of the γ-ray angular distribution was made by assuming that the alignment decays exponentially with time while the nucleus is in flight, but that the residual alignment at the moment of entry to the stopper is preserved thereafter. Details of the calculation can be found in Ref. 23. The exponential relaxation of alignment corresponds to the predictions of the theory due to Abragam and Pound[24] if the deorientation is caused by rapidly fluctuating random electromagnetic fields, such as might be expected from an atomic cascade. There are some difficulties with this approach. For example, the inferred correlation times of the fluctuating magnetic field are rather shorter than the expected lifetimes of atomic states.[25] Also, the exponential behavior is not correct near $t=0$. This second effect has been investigated in some detail,[26–29] but the deviations from exponential relaxation are small and, consequently, are very difficult to detect.[30] Thus the Abragam-Pound theory is, in general, very successful phenomenologically. A significant departure from exponential relaxation has been observed[31] in the decay of each of two isomers in ^{107}Cd. In these cases, the alignment relaxed with flight time to certain "hard-core" values and remained at those values for flight times as long as 7 ns. The hard-core alignments were appreciable, being about 40% of full alignment in one case and about 65% in the other. A hard-core alignment of 20% of full alignment has also been seen in the decay in vacuum of the first excited state of ^{150}Nd.[30]

Whether or not a significant hard core exists in the present data and what values of the relaxation times τ_k to use are questions which may be addressed by inspecting the variation of total γ-ray intensity with flight time. If all of the corrections are made properly, there should be no such variation. In Fig. 4 we show a plot of the

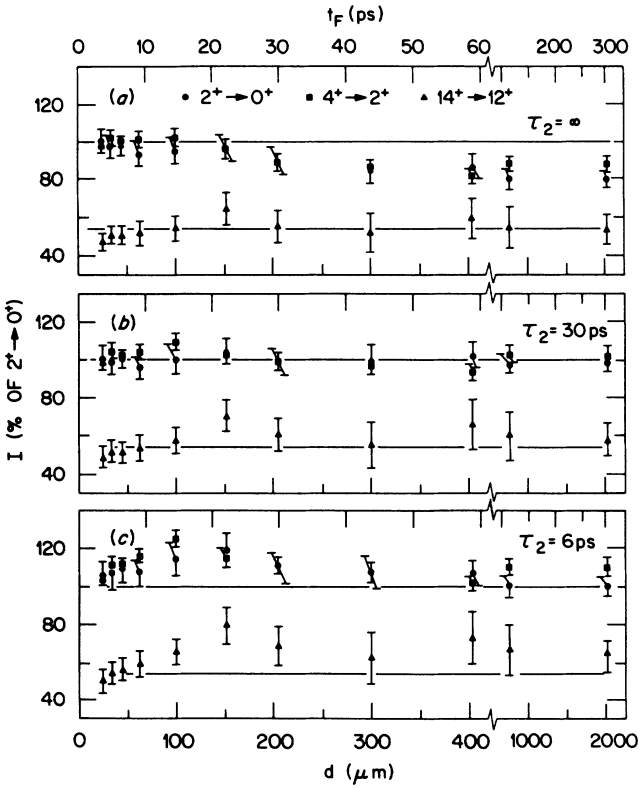

FIG. 4. The sum I of the shifted and unshifted peak intensities vs target-stopper separation d for three yrast transitions in ^{160}Yb, showing the effects of the correction for alignment attenuation. The correction is applied with (a) $\tau_2=\infty$, (b) $\tau_2=30$ ps, and (c) $\tau_2=6$ ps, and using $\tau_4=0.3\,\tau_2$.

sum I of the normalized shifted and unshifted γ-ray intensities of the $2^+ \rightarrow 0^+$, $4^+ \rightarrow 2^+$, and $14^+ \rightarrow 12^+$ transitions of ^{160}Yb versus recoil distance. The data are those obtained with the ^{48}Ti-induced reaction. Figure 4(a) shows the results when all corrections are applied except that for alignment attenuation. This is the same as setting τ_k infinite. In the case of the $2^+ \rightarrow 0^+$ transition, the intensity appears to be about 20% less for large recoil distances than for small distances, showing the attenuation of the alignment. The discrepancy is approximately $A_2 + A_4$, suggesting that there is no significant hard-core alignment. It is actually a little less than $A_2 + A_4$, but this is accounted for by the nonzero solid angle of the detector and the contribution of the shifted peak, which experiences less alignment attenuation than the unshifted peak. The effect of the shifted peak can be clearly seen in the results for the decay of the much shorter lived 4^+ and 14^+ states. In particular, the 14^+ state has no long-lived feeding and so shows no apparent loss of intensity at long flight times.

The effect of applying the alignment-attenuation correction with short relaxation times is shown in Fig. 4(c). The intensities at short to intermediate flight times are overcorrected. The relaxation times used ($\tau_2 = 6$ ps, $\tau_4 = 2$ ps) are those measured[32] in a recent experiment on ^{158}Dy and are apparently too short for the present case. Figure 4(b) shows that the values $\tau_2 = 30$ ps and $\tau_4 = 10$ ps give satisfactory results. Similar relaxation times have been measured in experiments[33] on ^{150}Sm and ^{156}Gd and have been found to be appropriate in the analysis of recoil-distance experiments on ^{150}Nd (Ref. 2) and ^{128}Ce (Ref. 20).

The values of τ_k are probably larger in the s band than in the ground-state band because of an expected reduction in g factors with the alignment of quasineutrons. However, the lifetimes and feeding times of the s-band states of ^{160}Yb are short enough for there to be little sensitivity to this effect. The results for the 14^+ state, the longest lived of the s-band states, shown in Fig. 4, indicate that the values of τ_k appropriate for the ground-state band are adequate for the analysis of the s band also.

In their analysis of recoil-distance data on ^{157}Dy, an isotone of ^{161}Yb, Emling *et al.*[3,4] omitted the alignment-attenuation correction on the grounds that the g factors of the high-spin states of odd-neutron nuclei are expected to be close to zero. We looked for a similar effect in ^{161}Yb by examining the inferred total intensity of the $\frac{17}{2}^+ \rightarrow \frac{13}{2}^+$ transition. Although the uncertainties are relatively large, it is clear that τ_2 values larger than 30 ps are preferred. We have used $\tau_2 = 300$ ps in the correction of the decay curves for ^{159,161}Yb.

The Abragam-Pound theory predicts that, if the randomly fluctuating deorientation field is purely magnetic, then $\tau_4 = 3\tau_2/10$. While deviations from this are well known,[33] they are not large enough to be significant for the analysis of this experiment, which is less sensitive to τ_4 than some other experiments (e.g., that of Ref. 2) because of the relatively small value of A_4.

As mentioned above, it has been assumed in the analysis of the data from the ^{116}Cd-induced reaction that the relaxation times are the same after passage through the retarding foil as before. A plot of the total intensity of the $4^+ \rightarrow 2^+$ γ rays against flight time shows that this assumption is adequate for our data.

2. *Line shape corrections*

Since the recoil does not stop instantaneously upon entering the stopper, or change its velocity instantaneously upon encountering the retarding foil, γ rays are emitted with intermediate Doppler shifts. These γ rays, which we treat as unshifted or less-shifted γ rays as the case may be, are lost in the extraction of the peak areas because of the high backgrounds present in γ-ray spectra from fusion-evaporation reactions. They are recovered by multiplying the unshifted or less-shifted peak areas by the ratio $U(t_F)/U(t_F + t_S)$, where t_F is the flight time of the recoils from the target to the front surface of the stopper or retarding foil, t_S is the stopping or slowing time, and $U(t)$ is the calculated intensity of the appropriate unshifted or less-shifted peak at flight time t. The calculation of $U(t)$ is described in Sec. III C. This correction, in common with the other corrections, must be applied iteratively, since estimates of lifetimes and feeding times are required to determine $U(t)$.

The slowing time t_S is determined by using the phenomenological stopping powers of Andersen and Ziegler[34] and of Ziegler.[35] A complication arises in that, for the case of an unshifted peak, a γ ray emitted from a sufficiently slowly moving recoil will have an undetectable Doppler shift and so will be counted in the unshifted peak. An analogous situation applies for less-shifted peaks. Hence t_S is taken as the time for the recoil to slow from its initial velocity to its final velocity (zero in the case of a stopper) minus an amount $c(\Delta E_\gamma / E_\gamma)$ corresponding to the resolution ΔE_γ of the γ-ray detector.

The line shape correction may be significant for those states whose lifetimes are comparable with or smaller than the slowing time. For the ^{116}Cd-induced reaction, the time taken to traverse the retarding foil was 0.17 ps, which is substantially smaller than any lifetime measurable in this experiment. The corrections to these data are, without exception, much smaller than the uncertainties from spectrum analysis. On the other hand, the recoils from the ^{48}Ti induced reaction took 1.0 ps to stop, leading to significant effects for some transitions.

C. Treatment of feeding

None of the levels observed in this experiment is directly populated by the reaction; rather, they are near the end of a decay cascade involving unobserved levels with appreciable lifetimes. Allowance for the time structure of this feeding is the principal problem of the analysis. We have addressed this by constructing a model of the decay scheme in question and by supposing that the population resides initially in hypothetical feeding levels. The population $P_i(t)$ of state i at a later time t is then found by solving Bateman's equations.[36,37]

The required shifted, unshifted, and less shifted inten-

sities follow from the model of the decay cascade and the values taken for $P_i(0)$ and the partial widths Γ_{ij} for the decay $i \rightarrow j$. In the analyses we use the computer program[23] LIFETIME developed from an original version supplied by Emling.[38] In our program, $P_i(0)$ and Γ_{ij} are varied to fit the experimental values of the intensities. The program also calculates and applies the corrections described in Sec. III B. This reduces the determination of $P_i(0)$ and Γ_{ij} to a problem of statistical inference, to which standard techniques[39,40] are applied. The question of choosing the model for the decay cascade remains. Clearly, one starts with the known levels and transitions. However, most levels decay with a greater intensity than is seen to populate them. The simplest way of providing this unseen sidefeeding is by a single hypothetical level whose initial population supplies the missing intensity. But this model is somewhat unphysical because it gives a sidefeeding rate which is highest at time $t=0$. Since the observed levels are not near the top of the cascade, one expects the sidefeeding rate to be zero at $t=0$ and to rise to some maximum value before falling away. The simplest way of obtaining this behavior is to stack two levels in cascade and give the lower one no initial population. In general, this model was adopted in the present work; it results in the sidefeeding into each level being described by three parameters: the initial population of the upper level of the sidefeeding cascade and the two lifetimes.

In a few cases—for example, the feeding into the top of the $h_{9/2}$ band of ^{161}Yb—a two-level sidefeeding cascade was found to be inadequate. This is because of the characteristic feature of two-level cascades that, if the effective decay constant at large times is Γ, then the maximum feeding rate, which coincides with the peak in the population of the lower level of the cascade, occurs farthest from $t=0$ when both levels have decay constants equal to Γ. In cases such as the above mentioned, it was necessary to add extra levels to the feeding cascade to obtain a feeding rate which peaked later than could be obtained with a two-level cascade with the appropriate behavior at large times. However, in all cases extracted lifetimes of the levels of interest were insensitive to the number of levels in the sidefeeding cascade.

The number of levels involved in ^{160}Yb is so large that it was not practical to vary all parameters simultaneously. Even if it were possible, it is not always desirable to do so because of the likelihood of the more precise decay curves at the bottom of the decay scheme unduly influencing χ^2. Instead, a strategy was developed in which groups of a few decay curves were fitted together to obtain the lifetimes of the lowest levels of the group. Where available and pertinent, branching ratios were included as additional data to be fitted.

IV. RESULTS

A. The nucleus ^{160}Yb

Decay curves were obtained for all transitions marked by solid arrows in Fig. 5. The flow of population is indicated by showing the sidefeeding intensity needed for the intensity balance at each level. In the following subsections the results are presented in detail.

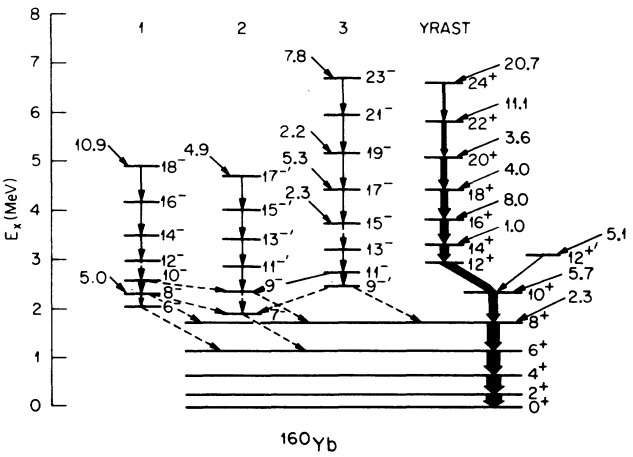

FIG. 5. A portion of the decay scheme of ^{160}Yb showing, by solid arrows, those transitions for which decay curves were obtained. The sidefeeding intensities are given as percentages of the $2^+ \rightarrow 0^+$ intensity.

1. Yrast transitions

We were unable to obtain a decay curve for the $26^+ \rightarrow 24^+$ transition because it is one member of an unresolved doublet. The $24^+ \rightarrow 22^+$ transition is the highest yrast transition for which a decay curve is available. However, in the absence of any information about the time structure of the feeding, we can only set an upper limit on the lifetime of the 24^+ state. This leaves the 22^+ state as the highest yrast state for which a lifetime can be obtained reliably.

Decay curves for the decay of yrast states are displayed in Fig. 6, which includes only those states for which lifetimes could be obtained. In addition to showing the intensity U or L of the unshifted or less shifted peaks as a function of flight time t_F, Fig. 6 also shows the difference between the total intensity I and the shifted intensity S against t_F. Since the shifted and unshifted or less shifted peaks are separately normalized, $I-S$ is a second, almost independent, measurement of U or L. The total intensity I includes the corrections described in Sec. III B and is well determined, being the average of $U+S$ (or $L+S$) at all flight distances, including those, not shown in Fig. 6, for which U, L, or $I-S$ is zero. Data from the ^{116}Cd-induced reactions were obtained for the decay of the 18^+ state and below, as shown in Fig. 6. As noted in Sec. II, these have been scaled by an overall normalization and shifted along the time axis.

The curves in Fig. 6 are the results of the fitting and correspond to the lifetimes τ and sidefeeding times τ_{feed} that are given in Table I. The sidefeeding times, which are the lifetimes of the lowest levels of the sidefeeding cascades, all have uncertainties of about 50% and are to be taken as representative only. Table I also lists sidefeeding intensities I_{feed} and transition quadrupole moments Q_t. The sidefeeding intensities are expressed as the percentage of the unobserved feeding intensity to

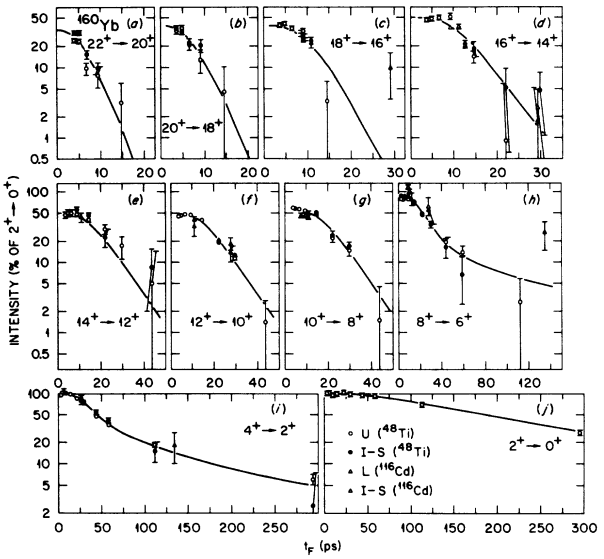

FIG. 6. Decay curves for the decay of the (a) 22^+, (b) 20^+, (c) 18^+, (d) 16^+, (e) 14^+, (f) 12^+, (g) 10^+, (h) 8^+, (i) 4^+, and (j) 2^+ states of ^{160}Yb. The points show values of the unshifted-peak intensity U, less-shifted-peak intensity L, and the total intensity minus the shifted-peak intensity $I-S$ after application of all corrections. The curves are fits as described in the text. In the legend, the beam used to induce the reaction is shown in parentheses.

the intensity of the depopulating γ ray. The transition quadrupole moments are related to the $B(E2; I \rightarrow I-2)$ values, obtained from τ in the usual way, by

$$B(E2; I \rightarrow I-2) = \frac{5}{16\pi} \langle I\,2\,K\,0 \mid I-2\,K \rangle^2 Q_t^2 \,. \quad (1)$$

We have assumed $K=0$ for these states. In calculating $B(E2)$ values, the internal conversion coefficients of Rösel *et al.*[41] were used.

Insofar as Q_t might be expected to vary smoothly along a collective band, the result for the 16^+ state is surprising. It is unlikely that this has been brought about by an error in correcting for sidefeeding, since the sidefeeding intensity is only 17% of the intensity of the $16^+ \rightarrow 14^+$ γ ray. It is true that the best-fit sidefeeding time, 5 ps, is rather long, but forcing this to be shorter does not change the inferred lifetime significantly. It is also unlikely that there has been an error in extracting the intensities of the $16^+ \rightarrow 14^+$ γ ray from the spectra, since the relevant lines occur in a particularly uncluttered part of the spectrum.

A previous measurement of the lifetimes of states in the ground-state band of ^{160}Yb has been made by Bochev *et al.*[42] who used an (^{40}Ar,4n) reaction. Their results are compared with ours in Table I. Although they did their work before the discovery[8] of the negative-parity sidebands of ^{160}Yb, it is surprising that they should have found the $10^+ \rightarrow 8^+$ and $8^+ \rightarrow 6^+$ transitions to be as intense as the lower γ rays. This is inconsistent both with the current work and with previous results.[8,9]

2. *The negative-parity sidebands*

Gamma rays from transitions in these bands are, in general, much weaker than those from the yrast cascade. Indeed, for the weakest of them (band 2 in Fig. 5), the decay curves of the higher transitions were not considered sufficiently reliable for obtaining lifetimes. They were fitted and used solely to provide additional information on the feeding into the 9^- level. Decay curves

TABLE I. Lifetimes, transition quadrupole moments, and sidefeeding intensities and times for some positive-parity states of ^{160}Yb.

State	E (keV)[b]	τ (ps)	Q_t (e b)	I_{feed} (%)	τ_{feed}[a] (ps)	Bochev *et al.*[c] τ (ps)	Bochev *et al.*[c] I_{feed} (%)
			s band				
24^+	795.6	<4					
22^+	736.4	1.4±0.5	2.7±0.5	35	2		
20^+	663.5	1.6±0.4	3.3±0.4	10	2		
18^+	578.2	3.2±0.5	3.3±0.3	10	4		
16^+	483.9	2.3±0.5	6.1±0.7	17	5		
14^+	404.0	9.6±0.8	4.7±0.2	2	9		
12^+	586.4	1.5±0.6	$4.8^{+1.4}_{-0.8}$	0			
			Ground-state band				
$12^{+\prime}$	763.7	<9					
10^+	636.8	1.5±0.8	$3.8^{+1.9}_{-0.7}$	10	6	0.9±0.5	100
8^+	589.2	2.1±0.7	4.1±0.7	3	10	1.3±0.5	0
6^+	508.5	<1.6	>6	0		2.7±0.3	0
4^+	395.4	14.8±1.0	4.40±0.16	0		11.6±0.6	0
2^+	243.2	159±9	5.13±0.15	0		182±6	0

[a]The uncertainties in the feeding times are about 50%.
[b]Transition energies have uncertainties of ±0.1 keV.
[c]Reference 42.

for other transitions are shown in Fig. 7, and inferred lifetimes, Q_t values, and sidefeeding intensities and times are given in Table II. The Q_t values were calculated under the assumption that $K=0$ for these bands. Once again, only limits can be obtained on the lifetimes of the topmost states seen in each band.

The 12^- and 15^- states are omitted from Table II because contaminating lines of about the same energies rendered the extraction of intensities unreliable. The rejection of the decay curve of the 15^- state leaves insufficient information about the feeding time to the 13^- state to be able to get a lifetime for that state. An upper limit can, however, be extracted from the $13^- \rightarrow 11^-$ decay curve. Our earlier reports[11-13] of this work quote a value for the lifetime of the 15^- state, which we now believe to be unreliable for the above reason. Despite the rejection of the $12^- \rightarrow 10^-$ decay curve, it is still possible to obtain the lifetime of the 10^- state, principally because it is long. Also, the intensity of the $10^- \rightarrow 8^-$ transition, taken with the previously measured branching ratios,[9] is consistent with the intensity of the $14^- \rightarrow 12^-$ transition, implying that there is negligible sidefeeding to either the 12^- or 10^- states. The value for the lifetime of the 10^- state does depend on the lifetime assumed for the 12^- state. We have used $\tau_{12^-}=13$ ps, corresponding to $Q_t=4.0$ e b. Halving or doubling this lifetime changes the lifetime of the 10^- state by ± 18 ps. This uncertainty is incorporated in the uncertainty given in Table II. The long lifetime of the 10^- state makes it impossible to obtain a lifetime for the 8^- state. Similarly, the lifetimes of the 9^- and 7^- states of band 2 and the $9^{-\prime}$ state of band 3 are submerged by the lifetimes of the 10^- and 11^- states.

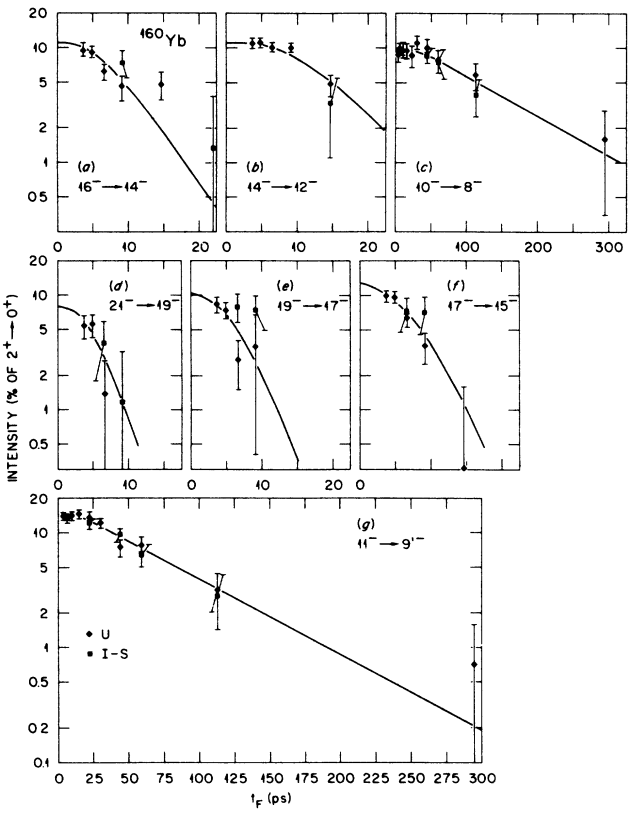

FIG. 7. Decay curves for the decay of the (a) 16^-, (b) 14^-, and (c) 10^- states of band 1 and the (d) 21^-, (e) 19^-, (f) 17^-, and (g) 11^- states of band 3 of ^{160}Yb. See the caption to Fig. 6 for details. The bands are identified in Fig. 5.

TABLE II. Lifetimes, transition quadrupole moments, and sidefeeding intensities and times for some negative-parity states of ^{160}Yb.

State	E_γ (keV)	τ (ps)	Q_t (e b)	I_{feed} (%)	τ_{feed} (ps)
		Band 1			
18^-	739.1	<7			
16^-	653.7	2.0 ± 1.0	$3.1^{+1.2}_{-0.6}$	0	
14^-	540.6	5.5 ± 1.8	3.0 ± 0.5	0	
10^-	216.4	130 ± 40[a]	5.4 ± 0.7	0	
		Band 2			
$17^{-\prime}$	673.7	<10			
$13^{-\prime}$	544.4	<4		0	
		Band 3			
23^-	746.3	<3			
21^-	770.6	2.4 ± 0.9	1.9 ± 0.3	0	
19^-	748.7	1.9 ± 1.1	$2.2^{+1.3}_{-0.4}$	22	1.3
17^-	671.6	2.1 ± 0.8	2.8 ± 0.5	34	<1
15^-	561.7	<5			
13^-	432.1	<8		13	<1
11^-	282.7	67 ± 6[b]	3.8 ± 0.20	0	

[a]The partial lifetime for the in-band $10^- \rightarrow 8^-$ transition is 140 ± 40 ps.
[b]The partial lifetime for the in-band $11^- \rightarrow 9^{-\prime}$ transition is 83 ± 9 ps.

The concept of transition quadrupole moment only applies to decays between members of a rotational band,[43] so the Q_t values shown in Table II for the 10^- and 11^- states were calculated using the partial lifetimes for the in-band decays. These are given at the foot of Table II.

B. The nuclei ^{159,161}Yb

As the products of side reactions, fewer transitions were observed from ^{159,161}Yb than from ^{160}Yb. The intensity diagrams are shown in Fig. 8, where the sidefeeding intensity is shown as a percentage of the intensity of the strongest transition in each band segment. Decay curves for the states of ^{159}Yb are shown in Fig. 9 and for states of ^{161}Yb in Fig. 10. The splitting of intensity at the $\frac{29}{2}^-$ state of ^{161}Yb (see Refs. 10 and 11), which decays in one of two ways, made it impossible to obtain decay curves in the region of the backbend. Also, the $\frac{25}{2}^- \rightarrow \frac{21}{2}^-$ (561.9 keV) transition forms a doublet with the $15^- \rightarrow 13^-$ transition of ^{160}Yb.

Lifetimes, transition quadrupole moments, and feeding parameters inferred from the decay curves of Figs. 9 and 10 are listed in Table III. To determine the Q_t values of these states, one needs to know the value of K. Although the bandheads of the three bands have all been identified with $K=\frac{1}{2}$ and $\frac{3}{2}$ Nilsson states, it is believed that the bands rapidly become aligned with increasing angular momentum, resulting in states of mixed K. But rotation-aligned states are dominated by components with low K, so it might be expected that the alignment process does not perturb the $B(E2)$ values significantly in these cases. The following calculation shows this to be so. For mixed-K states, Eq. (1) becomes

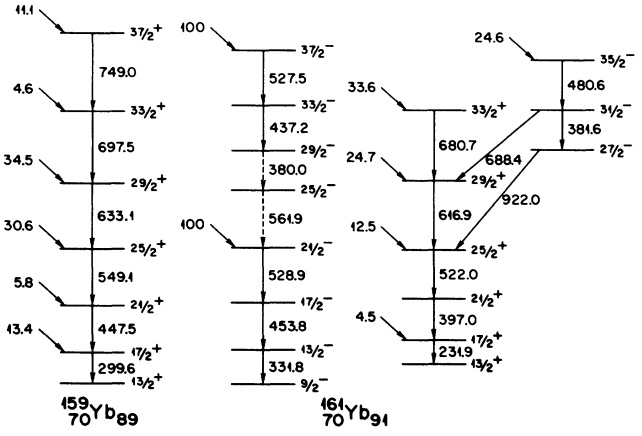

FIG. 8. Portions of the decay schemes of ^{159,161}Yb, showing, by solid lines, those transitions for which decay curves were obtained. Lifetimes of transitions in the negative parity band feeding the $i_{13/2}$ band were not measured, but these transitions were included in the modeling. The sidefeeding intensities are given as percentages of the intensity of the lowest transition in each band fragment.

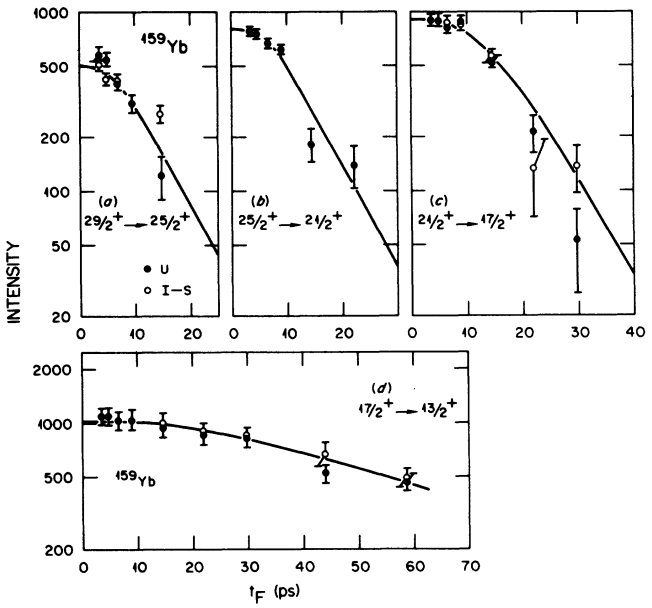

FIG. 9. Decay curves for the decays of the (a) $\frac{29}{2}^+$, (b) $\frac{25}{2}^+$, (c) $\frac{21}{2}^+$, and (d) $\frac{17}{2}^+$ states of ^{159}Yb. See the caption to Fig. 6 for details.

$$B(E2; I \rightarrow I-2) = \frac{5}{16\pi} Q_t^2 \times \left[\sum_k a_K(I) a_K(I-2) \times \langle I\, 2K\, 0 \mid I-2K \rangle \right]^2 , \quad (2)$$

where $a_K(I)$ are the expansion coefficients of the state of angular momentum I in terms of states of pure K. For a rotation-aligned state involving a single quasiparticle of angular momentum j, $a_K(I)$ is given[44] by

$$a_K(I) = d^j_{jK}\left[\frac{\pi}{2}\right] , \quad (3)$$

where $d^j_{mn}(\beta)$ is a reduced rotation matrix element. The positive-parity bands have $j=\frac{13}{2}$ and are based on the $\frac{1}{2}^+[660]$ and $\frac{3}{2}^+[651]$ Nilsson states for ^{159}Yb and ^{161}Yb, respectively. The negative-parity band is a mixture of predominantly $j=\frac{9}{2}$ and $\frac{7}{2}$ from the $\frac{3}{2}^-[521]$ and $\frac{3}{2}^-[532]$ Nilsson states. For each of these j values, the sum over K in Eq. (2) differs from

$$\langle I\, 2\, \tfrac{3}{2}\, 0 \mid I-2\, \tfrac{3}{2} \rangle^2$$

by no more than a few percent for the values of I of interest. Since this is much less than the experimental uncertainties, we have used Eq. (1) with $K=\frac{3}{2}$ to calculate the Q_t values in Table III, even for the $\frac{33}{2}^-$, three quasiparticle state.

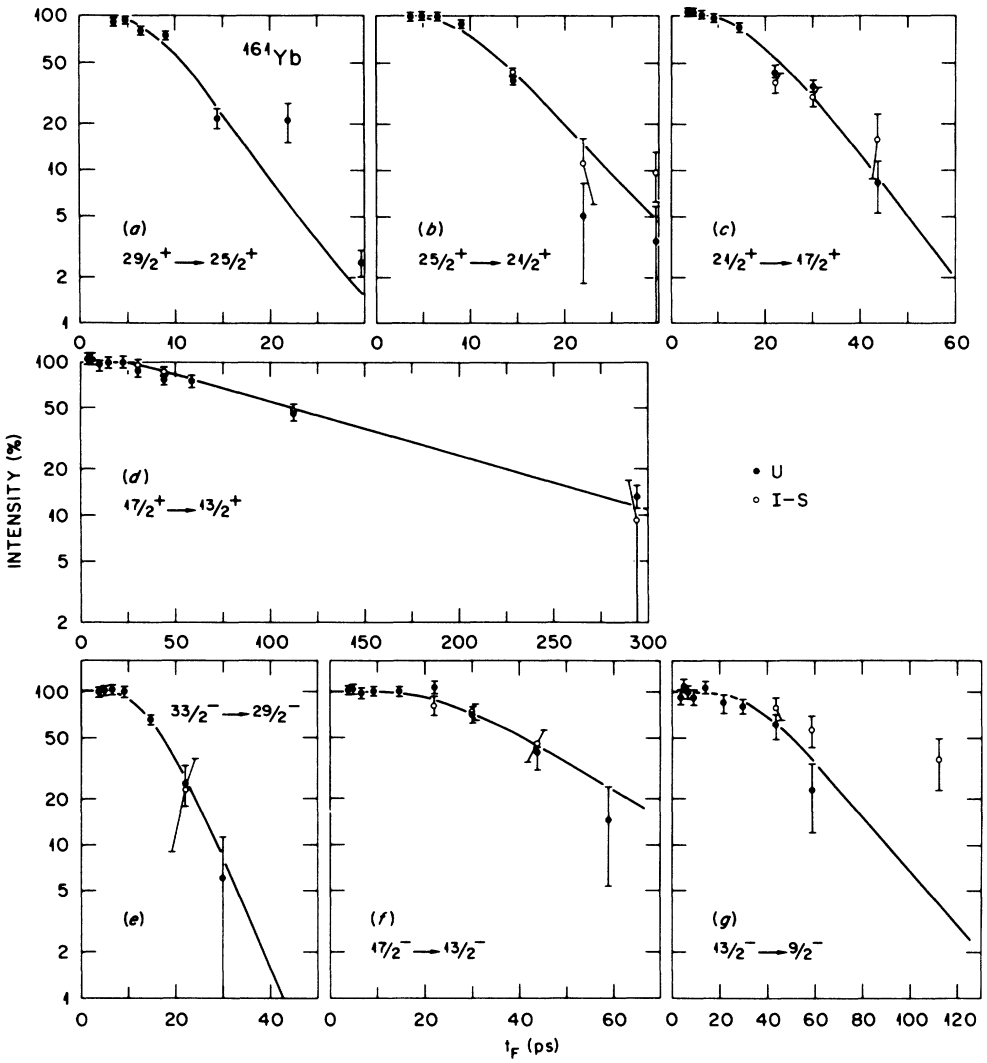

FIG. 10. Decay curves for the decay of the (a) $\frac{29}{2}^+$, (b) $\frac{25}{2}^+$, (c) $\frac{21}{2}^+$, (d) $\frac{17}{2}^+$, (e) $\frac{33}{3}^-$, (f) $\frac{17}{2}^-$, and (g) $\frac{13}{2}^-$ states of ^{161}Yb. See the caption to Fig. 6 for details.

V. DISCUSSION

The Q_t values in Table I show that the high-spin states of ^{160}Yb have substantially lower Q_t values than do the 2^+ and 4^+ states. It is pertinent to ask whether this is due simply to the alignment of quasiparticles or whether there is some other process operating. Also, if alignment does play a part, does the effect depend on the orbitals to which the quasiparticles belong? The first part of this section examines these questions from a purely phenomenological point of view. In the second part, the discussion is widened to the systematics of other $N=89-91$ nuclei. The final part discusses the theoretical interpretation of the data for ^{160}Yb.

A. Phenomenology

The Q_t values listed in Tables I and II are plotted against rotational frequency $\hbar\omega$ in Fig. 11. The definition of rotational frequency in Ref. 1 is used, with the assumptions that $K=0$ for states of ^{160}Yb and $K=\frac{3}{2}$ for the odd mass nuclei. The ground-band states of ^{160}Yb [Fig. 11(b)] do not show the smooth centrifugal stretching characteristic of other $N=90$ nuclei, but instead suggest a slight decrease of Q_t with rotational frequency. This is discussed further in Sec. V B, where the systematics is presented.

The most striking feature of Fig. 11 is the decrease of Q_t with increasing rotational frequency that is exhibited by the bands with aligned quasiparticles. This is most clearly seen in the s-band states, apart from the anomalous 16^+ state, and negative-parity states of ^{160}Yb, and in the $i_{13/2}$ states of ^{161}Yb. The details of the effect are open to argument, however. The Q_t values for ^{159}Yb [Fig. 11(a)] seem to be constant up to $\hbar\omega\sim0.27$ MeV followed by a sharp decrease. The same applies to the data for ^{161}Yb shown in Fig. 11(d). On the other hand, the Q_t values of the negative parity bands of ^{160}Yb, shown in Fig. 11(c), seem to vary smoothly with $\hbar\omega$, although a

TABLE III. Lifetimes, transition quadrupole moments, and sidefeeding intensities and times for some states of ^{159,161}Yb.

State	τ (ps)	Q_t (e b)	I_{feed} (%)	τ_{feed} (ps)
		^{159}Yb, $i_{13/2}$ band		
$\frac{37}{2}^+$	<13			
$\frac{33}{2}^+$	<1.7		29	3
$\frac{29}{2}^+$	3.4±1.1	2.6±0.4	69	4
$\frac{25}{2}^+$	2.1±0.6	4.8±0.8	38	4
$\frac{21}{2}^+$	5.4±0.8	5.0±0.4	7	7
$\frac{17}{2}^+$	45±6	4.7±0.3	13	20
		^{161}Yb, $i_{13/2}$ band		
$\frac{33}{2}^+$	<2			
$\frac{29}{2}^+$	2.3±0.5	3.4±0.4	36	2
$\frac{25}{2}^+$	2.2±0.4	$5.2^{+0.7}_{-0.5}$	0	
$\frac{21}{2}^+$	10.4±0.8	4.87±0.23	0	
$\frac{17}{2}^+$	123±8	5.21±0.20	3	3
		^{161}Yb, $h_{9/2}$ band		
$\frac{37}{2}^-$	<4			
$\frac{33}{2}^-$	6.0±1.1	4.9±0.4	0	
$\frac{21}{2}^-$	<30			
$\frac{17}{2}^-$	5±3	$5.3^{+3.1}_{-1.2}$	0	
$\frac{13}{2}^-$	9±5	$8.7^{+4.1}_{-1.6}$	0	

description in terms of a constant Q_t for the 14^- to 21^- states with a sharply rising Q_t at lower $\hbar\omega$ is not impossible. The s band of ^{160}Yb [Fig. 11(b)] shows a more complex behavior, with the Q_t value of the 16^+ state being well above the general trend. If one neglects this value, then either a linear dependence, as shown in Fig. 11(b) or a constant Q_t for the 18^+, 20^+, and 22^+ states with a sharp rise to the 14^+ state could be postulated.

Both of the suggested forms for the variation of Q_t with $\hbar\omega$, namely the linear dependence and the rapid change from a constant value, give similar results near $\hbar\omega \sim 0.3$ MeV in all of the cases shown in Fig. 11. This raises the possibility of comparing the collectivity of the various bands at about that rotational frequency. One finds $Q_t \sim 3.4\ e$ b for the s band of ^{160}Yb and $Q_t \sim 2.9\ e$ b for the negative-parity bands of that nucleus. To minimize the effect of the local variation of Q_t with mass, these numbers should be compared with the mean of the values for the two odd-mass nuclei. At $\hbar\omega = 0.3$ MeV, $Q_t \approx 3.4\ e$ b for ^{159}Yb and $Q_t \approx 3.6$ MeV for ^{161}Yb, giving a mean of about 3.5 e b. The quasiparticles involved in these bands are the two lowest-energy $i_{13/2}$ quasineutrons, known as A and B, and the two lowest-energy negative-parity quasineutrons (mainly of $h_{9/2}$ and $f_{7/2}$ character), known as E and F. In the odd-mass nuclei, the bands shown in Fig. 11 are built on quasiparticle A; in ^{160}Yb, the s band involves the AB pair, and the negative-parity bands involve the AE and AF pairs. The similarity of the Q_t values at $\hbar\omega = 0.3$ MeV for all of these bands suggests that the variation of Q_t with rotational frequency is principally caused by the common quasiparticle, that is, quasiparticle A. The $\frac{33}{2}^-$ state of ^{161}Yb is a member of the three-quasiparticle band ABE. Its Q_t value also suggests that the effect of quasiparticle A dominates that of quasiparticles B and E.

B. Systematics

In the first part of this section, the behavior of the ground-state bands of $N = 90$ nuclei is considered. The second part examines the conclusions of the preceding section in the light of results for other $N = 89$–91 nuclei. Only even-Z nuclei are considered in order to avoid the complication of an unpaired proton. (There exist extensive data[45] on lifetimes of states of the $N = 90$ nucleus ^{157}Ho. These seem to show little variation with spin and therefore with rotational frequency.)

1. Zero-quasiparticle bands

Transition quadrupole moments are now available for the ground-state bands of six $N = 90$ nuclei. These are shown in Fig. 12. Starting with the lightest of these nuclei, the average Q_t increases with increasing Z until

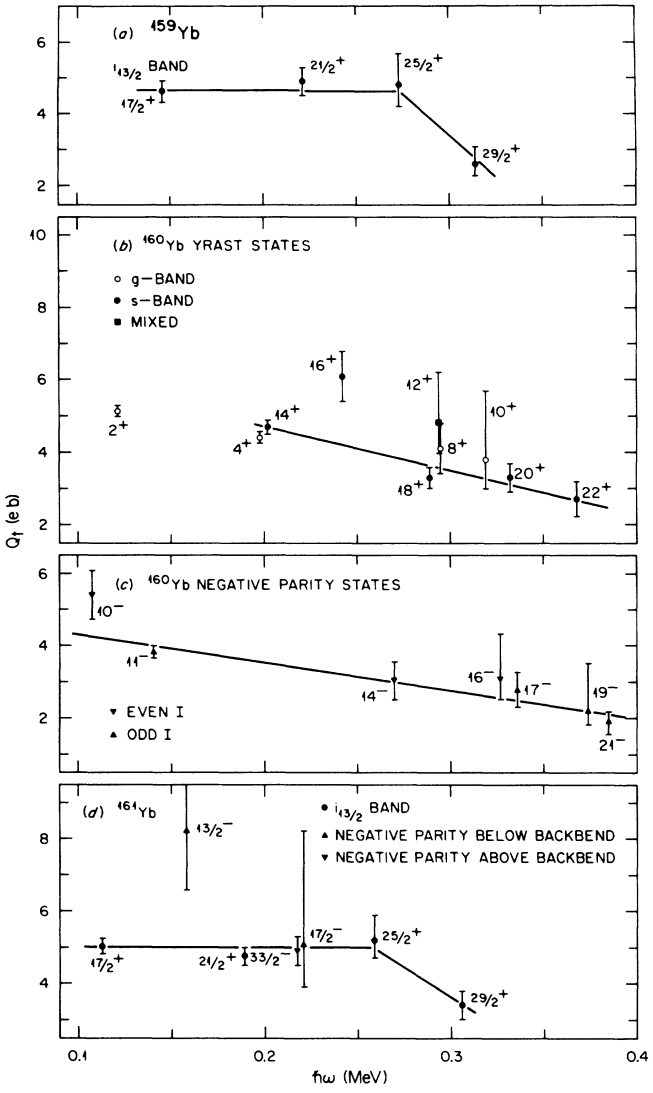

FIG. 11. Transition quadrupole moments Q_t vs rotational frequency $\hbar\omega$ for (a) states of ^{159}Yb, (b) yrast states of ^{160}Yb, (c) negative-parity states of ^{160}Yb, and (d) states of ^{161}Yb. In (a) and (d) the solid lines are visual fits to the trends in the data. The solid line in (b) is a least squares fit to the s-band states, excluding the 16^+ member. The solid line in (c) is a least squares fit to all of the data shown. The trends represented by the solid lines are discussed in the text.

^{154}Gd and ^{156}Dy are reached, where the trend is reversed. This reflects the position of dysprosium at the middle of the $Z=50-82$ proton shell.

The lighter nuclei show a trend of increasing Q_t values with increasing rotational frequency. This has been interpreted as centrifugal stretching, the detailed mechanism being the mixing of the ground, beta, and gamma bands by the rotation-vibration interaction. If this interaction is assumed to be small, then one obtains[57]

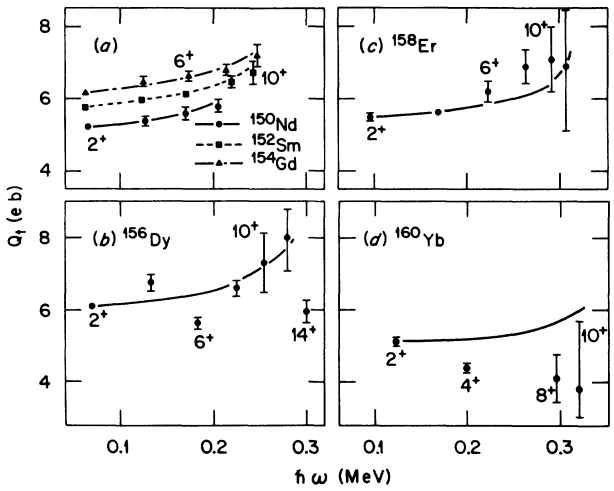

FIG. 12. Transition quadrupole moments Q_t vs rotational frequency $\hbar\omega$ for the ground-state bands of $N=90$ nuclei. The data are weighted means of the results of ^{150}Nd (Refs. 2, 46, and 47), ^{152}Sm (Ref. 48), ^{154}Gd (Refs. 49 and 50), ^{156}Dy (Refs. 3, 4, 21, 51, and 52), ^{158}Er (Refs. 5 and 53–56), and ^{160}Yb (present work). The lines are predictions of a simple band-mixing model described in the text.

$$Q_t(I^\pi)=Q_t(2^+)[1+\alpha(I^2-I-2)]\,, \tag{4}$$

where α is here taken as an adjustable parameter.[56] The curves in Fig. 12 show the predictions of Eq. (4) with $Q_t(2^+)$ taken from the data and α set to 0.002 (Refs. 21, 58, and 59), except for ^{150}Nd, for which $\alpha=0.0026$ (Ref. 2). It can be seen that this simple model describes the lightest three nuclei in Fig. 12 very well. However, the data for ^{156}Dy oscillate about the line, the 4^+ state being high and the 6^+ state low. (It is emphasized that the lifetimes of these two states have been measured by two different groups,[3,4,21] and the results agree.) Erbium-158 is fairly well described by centrifugal stretching, but ^{160}Yb is not; in this case the 4^+ state is low. Equation (4) breaks down at high spin since the rotation-vibration interaction is no longer small. This effect has been seen in ^{156}Dy, where Q_t values are available[3,4] for ground-state-band states up to $I=24$. [Results for the higher-spin ground-state band states have been omitted from Fig. 12(b).]

2. *One- and two-quasiparticle bands*

Extensive measurements of the lifetimes of states in aligned bands are available for ^{156,157}Dy (Refs. 3, 4, and 21) and ^{157,158,159}Er (Ref. 5). These are shown in Fig. 13. For the other isotones, few lifetimes that can yield Q_t values have been measured; those that are available pertain to relatively low-spin states at low rotational frequency in the odd-mass nuclei. The degree of alignment of these states is probably not high and these data are not shown. The Q_t and $\hbar\omega$ values for the odd-mass nuclei have all been calculated assuming $K=\frac{3}{2}$.

The data in Fig. 13 for the three odd-mass nuclei and for the s bands of the two $N=90$ nuclei all show evi-

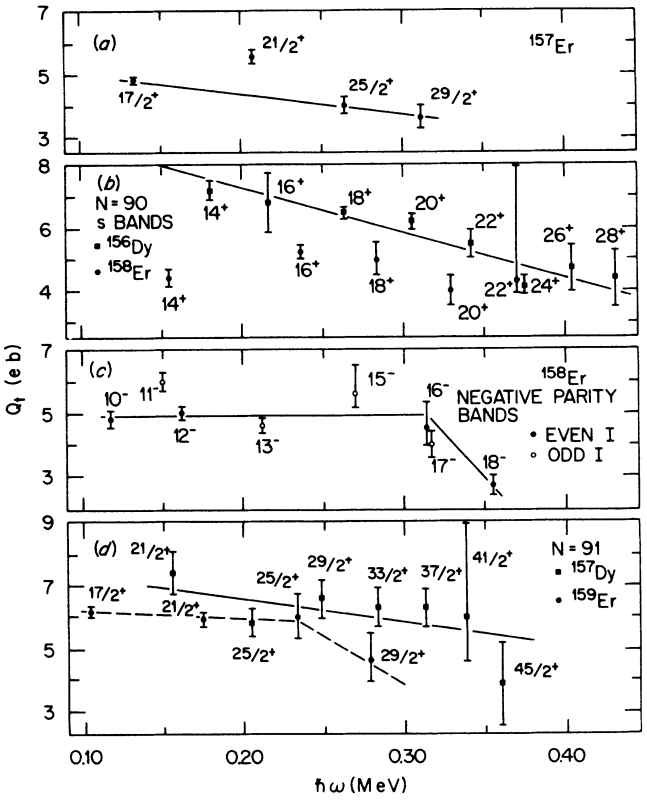

FIG. 13. Transition quadrupole moments Q_t vs rotational frequency $\hbar\omega$ for (a) ^{157}Er, (b) the s bands of ^{156}Dy and ^{158}Er, (c) negative parity states of ^{158}Er, and (d) ^{157}Dy and ^{159}Er. The data are weighted means of the results of ^{156}Dy (Refs. 3, 4, and 21), ^{157}Dy (Refs. 3 and 4), ^{157,159}Er (Refs. 5 and 56), and ^{158}Er (Refs. 5, 54, and 55). The solid lines are discussed in the text. The dashed line in (d) seems to best represent the trend of the ^{159}Er data.

dence for a frequency dependence of Q_t. In each case the dependence could either be smooth or constant with a rapid change at an appropriate frequency. There are several data which do not follow the general trend. For example, the Q_t of the $\frac{21}{2}^+$ state of ^{157}Er is large; if it is neglected, then the remaining Q_t values show a smooth behavior with $\hbar\omega$. In ^{158}Er, the Q_t of the 14^+ state is low, but this is probably due to mixing with the ground-state band. In ^{157}Dy the Q_t of the $\frac{25}{2}^+$ state is also low. For ^{159}Er the Q_t values are best described by a constant value below $\hbar\omega \approx 0.23$ MeV with a decrease thereafter. The Q_t values for the negative-parity bands of ^{158}Er are somewhat scattered, but are not inconsistent with the postulate of frequency dependence as indicated by the solid line in Fig. 13(c). The even-spin states seem to have constant Q_t below $\hbar\omega \approx 0.31$ MeV. The data for the odd spin states are less regular.

The available data on $^{159-161}$Yb support the conclusion that the transition quadrupole moments of states in bands with aligned quasiparticles show a dependence on rotational frequency, with a tendency toward lower values at higher rotational frequencies. Whether the decrease is smooth or rather abrupt seems to depend on the particular case. We point out that all of the bands represented in Fig. 13 involve the quasiparticle A, supporting the suggestion that it is this quasiparticle which is responsible for the effect. It would be interesting to consider the behavior of a band which does not contain quasiparticle A, but such data are not available.

C. Theoretical interpretation

1. *Self-consistent models*

The equilibrium deformation parameters ε_2, γ of ^{160}Yb have been calculated as a function of rotational frequency by both the cranked Hartree-Fock-Bogoliubov[15,16] and cranked Nilsson-Strutinsky[60] methods. The deformation parameters ε_2 and γ can, under certain conditions, be related to Q_t by[43]

$$Q_t = \left[\frac{12}{5\pi}\right]^{1/2} ZeR_0^2 \varepsilon_2 \cos(30^\circ + \gamma) , \tag{5}$$

where R_0 is taken as $1.2A^{1/3}$ fm and Z, A are the atomic and mass numbers of the nucleus.

Figure 14(a) shows the values of ε_2, γ predicted in Refs. 15, 16, and 60. The Q_t values obtained from these with Eq. (5) are shown in Fig. 14(b) along with the experimental values. The calculations, on the average, get Q_t about right, but the details of the observed behavior of Q_t with spin are not predicted. For example, consider the calculations of Bengtsson *et al.*[15] The Q_t values predicted for the ground-state band increase with spin, whereas the experimental values tend to decrease with spin. In the s band the calculations predict a reduction in Q_t, but show very little variation with increasing spin. The latter effect arises because the increase in γ is offset by a small increase in ε_2.

The low values of Q_t observed for the 20^+ and 22^+ states of ^{160}Yb are at considerable variance with the calculations of ε_2 and γ. All of the calculations suggest that, for these spin values, ε_2 should be about 0.2. The observed Q_t values of about 3 e b would then require $\gamma \sim 25°$, should all of the effect be attributed to that degree of freedom. However, this is a much greater degree of triaxiality than is expected at such modest values of angular momentum.

Alternatively, if one takes $\gamma = 10°$, as suggested by Bengtsson *et al.*,[15] then it is necessary to reduce ε_2 to 0.15 in order to obtain a Q_t of 3 e b. The calculations of Tanabe and Sugawara-Tanabe[16] do suggest that, between spins 24 and 48, the principal change in deformation is one of reducing ε_2 with increasing angular momentum. They agree, however, with Bengtsson *et al.*[15] in expecting ε_2 to be roughly constant at lower spins. A similar result is obtained by Åberg,[60] using the cranked Nilsson-Strutinsky model. (Åberg quotes $\gamma = 118°$ for the ground state, but this is equivalent to $\gamma = -2°$ since, at zero cranking frequency, there is no distinction between the two prolate axes. Accordingly, we show $Q_t = 4.3$ e b in Fig. 14 as the result of this model for $I = 0$.)

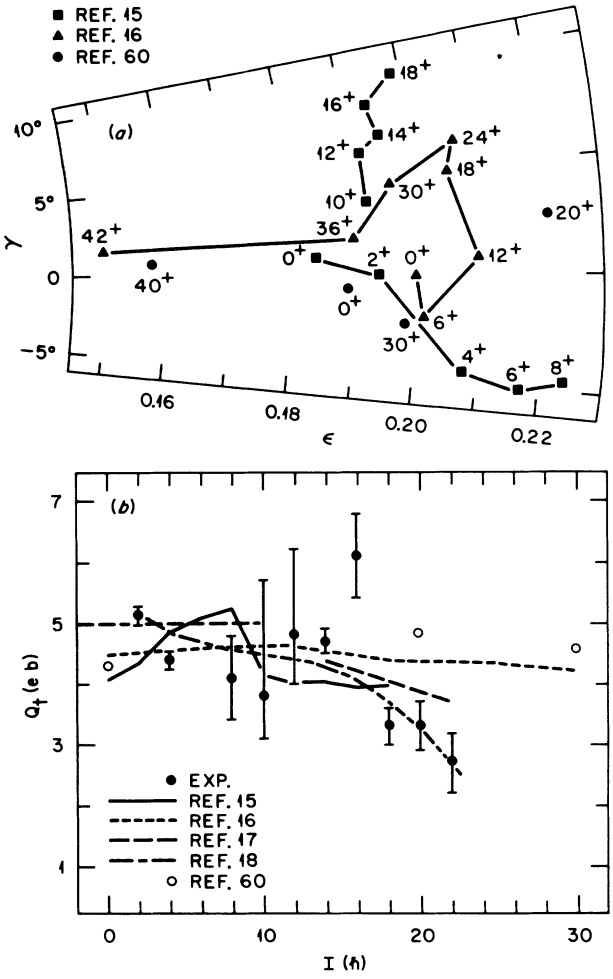

FIG. 14. (a) Calculated values of ε and γ from Refs. 15, 16, and 60; (b) transition quadrupole moments derived from these and from experiment, along with values calculated by the cranked shell model (Ref. 17) and by the fermion dynamical symmetry model (Ref. 18).

A partial explanation of the low Q_t values may lie in the approximations involved in the derivation of Eq. (5). One of the conditions for the validity of Eq. (5) is that γ be small. The cases considered in detail by Ring *et al.*[43] suggest that, for large magnitudes of γ, Eq. (5) may overpredict Q_t. If this were to occur here, then its correction would bring theory and experiment closer together. However, the effect is expected to be small at high spin, and it seems most unlikely that it can fully account for the present discrepancy.

2. *The cranked shell model*

One of the most widely used and successful models of nuclear behavior at high spin is the cranked shell model.[1] Deformations are not calculated by this model; rather, they are inserted *ab initio* as parameters. It is interesting that the success of the cranked shell model[1,9] has been achieved largely with deformations which are axially symmetric, independent of rotational frequency, and set at values appropriate to the ground state. These assumptions are brought into question by the present results. However, the cranked shell model has been extended to include triaxial shapes[61] and applied to odd-odd nuclei in the rare-earth region.[62] This study concludes that γ values as large as 25° may indeed occur at modest spins in this region. As to the details of the effect of alignment on collectivity, a study of the energy of aligned quasiparticles as a function of deformation[61] makes it clear that quasiparticle A should have a significant effect on the deformation of a soft core. However, it seems that the cranked shell model does not predict a reduction of Q_t with increasing rotational frequency. The calculations of Chen *et al.*[17] suggest that, in the region of ^{160}Yb, a band based purely on the AB pair of quasiparticles should show Q_t values which are independent of rotational frequency. Chen *et al.* explain the reduction in Q_t with rotational frequency observed in the s band of ^{160}Yb as being due to a gradual alignment with increasing rotational frequency of the EF pair. This effect, which amounts to a crossing of the AB and $ABEF$ bands with a very strong interaction between them, had previously been inferred[9,63] from the observed gradual increase with increasing rotational frequency in the alignment of the s band of ^{160}Yb. However, such an argument cannot be applied to other bands. For example, the negative parity bands of ^{160}Yb (bands 1 and 3 in Fig. 5) and the $i_{13/2}$ band of ^{161}Yb show no increase in alignment with increasing rotational frequency, yet they do show a decrease in Q_t.

3. *The fermion dynamical-symmetry model*

Another approach to the description of quadrupole collectivity at high spins has recently been suggested by Guidry *et al.*[18,64] This is based on a fermion dynamical-symmetry model of Wu *et al.*[65] The assumptions given in Ref. 18 lead to an analytical solution to the spherical shell model. This has been applied to ^{160}Yb, with the results[18] shown in Fig. 14(b). The calculation assumes an SU(3) fermion symmetry, which is expected to be only approximately correct for ^{160}Yb. In particular, symmetry-breaking terms important at the first backbend have been omitted, so that the results are probably not reliable in the region of spin 12–16. Notwithstanding this, the calculation is in reasonable agreement with the measured ground-state-band transition moments, and it also correctly predicts the observed decline of $E2$ strength above spin 16.

In the fermion dynamical-symmetry model, the loss of collectivity up a multiquasiparticle band is a general phenomenon resulting from the interplay between the angular momentum carried by a coherent core of fermion pairs with an SU(3) symmetry and that carried by broken fermion pairs. The coherent core loses $E2$ strength when forced to carry too much angular momentum. This loss of quadrupole collectivity has now been observed in the multiquasiparticle bands of many nuclei,[18] sometimes in contradiction to the initial predictions of cranking-type calculations. So, although calcu-

lations have not been performed either for the odd mass nuclei ^{159,161}Yb or for the negative-parity states of ^{160}Yb, the simple physics of the model suggests that the $E2$ strength in these cases should behave similarly to that of the s band of ^{160}Yb. This is just as the data above shows.

Since the fermion dynamical-symmetry model is a solution of the spherical shell model in the laboratory reference frame, it does not employ deformation parameters. Thus, although the loss of $E2$ collectivity may be accompanied by phenomena interpretable as the alignment of quasiparticles or excursions into the γ plane, the fermion dynamical-symmetry model, adopting the viewpoint of the spherical shell model, regards these effects as symptoms rather than causes. The cause of both of the latter effects plus the loss of $E2$ strength is, according to the fermion dynamical-symmetry model, the finite angular-momentum content of the shell-model collective subspace (coherent S-D core).

The fermion dynamical-symmetry model also suggests a possible explanation for the fluctuating Q_t values observed in the ground-state band. Such oscillations can arise from the effects of Coriolis antipairing. This has not been included in the calculation shown in Fig. 14(b), but the effect has been seen in ^{232}Th (Ref. 64). It remains to be seen whether the fermion dynamical-symmetry model can give a quantitative description of the observed fluctuations in the ground-state band of ^{160}Yb.

VI. SUMMARY

The recoil-distance method has been applied to evaporation residues from the reaction of ^{48}Ti plus ^{116}Cd. Both the "normal" and "inverse" reactions were studied at a center-of-mass energy of 145 MeV. Deexcitation γ rays were collected in coincidence with a total-energy filter to provide some discrimination on reaction channel. Decay curves were obtained for the yrast states of ^{160}Yb below $I=26$, and for many negative-parity states of that nucleus. Decay curves were also obtained for states of ^{159,161}Yb. The usual corrections were applied to the decay curves, with particular attention to the corrections for alignment attenuation and the line shape of the unshifted peaks. The decay curves were analyzed by modeling the decay scheme and applying Bateman's equations to the model.

The resulting transition quadrupole moments show the following behavior. The ground-state band of ^{160}Yb does not exhibit centrifugal stretching; rather, the Q_t values for the states of this band tend to decrease with spin. The Q_t values of states of the aligned bands of ^{159,160,161}Yb all show a dependence on rotational frequency with a tendency to decrease with increasing rotational frequency. This behavior seems to be related to the alignment of quasiparticle A. The available data from the isotones of ^{160,161}Yb are consistent with this.

Self-consistent calculations of the deformation of ^{160}Yb as a function of angular momentum are qualitatively consistent with the data, but have difficulty in reproducing the details. In particular, the observed reduction of Q_t with increasing angular frequency is not reproduced. Calculations with the cranked shell model indicate that quasiparticle A should have the dominant influence on the deformation of the nucleus, but provide an explanation of the variation of Q_t with frequency only for the case of the s band of ^{160}Yb. On the other hand, the fermion dynamical-symmetry model seems to give a general explanation for the observed behavior of Q_t with frequency. However, the calculations presented for rare-earth nuclei in the fermion dynamical symmetry model are not fully microscopic; so it remains to be seen whether the dynamical symmetry model can reproduce the full range of data to which the cranking model has been applied.

ACKNOWLEDGMENTS

We warmly thank H. Emling for supplying his computer code for the analysis of recoil-distance data. This served as the starting point for the development of our code. We also thank G. Leander, S. Frauendorf, R. Bengtsson, Y.-S. Chen, and J.-Y. Zhang for fruitful exchanges. One of us (S.C.P.) acknowledges a Fulbright travel grant by the U.S. Educational Foundation in India. Another of us (M.P.F.) acknowledges the support of the Department of Nuclear Physics, Australian National University, during the period in which much of this paper was written. Oak Ridge National Laboratory is operated by Martin Marietta Energy Systems, Inc. for the U.S. Department of Energy under Contract No. DE-AC05-84OR21400. Research at the University of Tennessee is supported by the U.S. Department of Energy under Contract No. DE-AS05-76ER04936.

*Present address: Department of Physics, University of New England, Armidale, New South Wales 2351, Australia.

†Present address: University of Jyväskylä, SF-40720 Jyväskylä 72, Finland.

‡On leave from Centre de Recherches Nucléaires, Strasbourg, France. Present address: GANIL, Boite Postal 5027, 14021 Caen Cedex, France.

[1]R. Bengtsson and S. Frauendorf, Nucl. Phys. **A314**, 27 (1979); **A327**, 139 (1979).

[2]S. W. Yates, N. R. Johnson, L. L. Riedinger, and A. C. Kahler, Phys. Rev. C **17**, 634 (1978).

[3]H. Emling, E. Grosse, D. Schwalm, R. S. Simon, H. J. Wollersheim, D. Husar, and D. Pelte, Phys. Lett. **98B**, 169 (1981).

[4]H. Emling, E. Grosse, R. Kulessa, D. Schwalm, and H. J. Wollersheim, Nucl. Phys. **A419**, 187 (1984).

[5]M. Oshima, N. R. Johnson, F. K. McGowan, C. Baktash, I. Y. Lee, Y. Schutz, R. V. Ribas, and J. C. Wells, Phys. Rev. C **33**, 1988 (1986).

[6]L. H. Courtney, M. P. Carpenter, A. J. Larabee, J. L. Riedinger, C. Baktash, M. L. Halbert, D. C. Hensley, N. R. Johnson, I. Y. Lee, M. Oshima, R. Ribas, Y. Schutz, L.

Adler, K. Honkanen, and D. G. Sarantites, Bull. Am. Phys. Soc. **30**, 761 (1985).
[7]J. Simpson, in Proceedings of the XXIIIrd International Winter Meeting on Nuclear Physics, Bormio, 1985.
[8]L. L. Riedinger, O. Anderson, S. Frauendorf, J. D. Garrett, J. J. Gaardhøje, G. B. Hagemann, B. Herskind, Y. V. Makovetsky, J. C. Waddington, M. Guttormsen, and P. O. Tjøm, Phys. Rev. Lett. **44**, 568 (1980).
[9]L. L. Riedinger, Nucl. Phys. **A347**, 141 (1980); Phys. Scr. **T5**, 36 (1983).
[10]J. J. Gaardhøje, Ph.D. thesis, University of Copenhagen, 1980.
[11]N. R. Johnson, in *Proceedings of the INS International Symposium on the Dynamics of Nuclear Collective Motion,* Mt. Fuji, 1982, edited by K. Ogawa and K. Tanabe (University of Tokyo, Tokyo, 1982), p. 144.
[12]M. P. Fewell, C. Baktash, M. W. Guidry, J. S. Hattula, N. R. Johnson, I. Y. Lee, F. K. McGowan, H. Ower, S. C. Pancholi, L. L. Riedinger, and J. C. Wells, in *Proceedings of the Conference on High Angular Momentum Properties of Nuclei,* Vol. 4 of *Nuclear Science Research Conference Series,* edited by N. R. Johnson (Harwood Academic, New York 1983), p. 69.
[13]M. P. Fewell, N. R. Johnson, F. K. McGowan, J. S. Hattula, I. Y. Lee, C. Baktash, Y. Schutz, J. C. Wells, L. L. Riedinger, M. W. Guidry, and S. C. Pancholi, Phys. Rev. C **31**, 1057 (1985).
[14]J. C. Wells, N. R. Johnson, F. K. McGowan, M. P. Fewell, J. S. Hattula, I. Y. Lee, C. Baktash, Y. Schutz, L. L. Riedinger, M. W. Guidry, and S. C. Pancholi, Bull. Am. Phys. Soc. **30**, 761 (1985).
[15]R. Bengtsson, Y.-S. Chen, J.-Y. Zhang, and S. Åberg, Nucl. Phys. **A405**, 221 (1983).
[16]K. Tanabe and K. Sugawara-Tanabe, Phys. Lett. **135B**, 353 (1984).
[17]Y. S. Chen. S. Frauendorf, and L. L. Riedinger, Phys. Lett. B **171**, 7 (1986).
[18]M. W. Guidry, C.-L. Wu, Z.-P. Li, D. H. Feng, and J. N. Ginocchio, Phys. Lett. B **187**, 210 (1987).
[19]N. R. Johnson, J. W. Johnson, I. Y. Lee, J. E. Weidley, D. R. Haenni, and J. R. Tarrant, Oak Ridge National Laboratory Physics Division Progress Report (Nov. 1981) ORNL-5787, p. 147.
[20]J. C. Wells, N. R. Johnson, J. Hattula, M. P. Fewell, D. R. Haenni, I. Y. Lee, F. K. McGowan, J. W. Johnson, and L. L. Riedinger, Phys. Rev. C **30**, 1532 (1984).
[21]D. Ward, H. R. Andrews, O. Häusser, Y. El Masri, M. M. Aléonard, I. Y. Lee, R. M. Diamond, F. S. Stephens, and P. A. Butler, Nucl. Phys. **A332**, 433 (1979).
[22]R. J. Sturm and M. W. Guidry, Nucl. Instrum. Methods **138**, 345 (1976).
[23]J. C. Wells, M. P. Fewell, and N. R. Johnson, Oak Ridge National Laboratory (ORNL) Technical Memo ORNL/TM-9105, 1985 (unpublished).
[24]A. Abragam and R. V. Pound, Phys. Rev. **92**, 943 (1953).
[25]G. Goldring, N. Hagemeyer, N. Benczer-Koller, R. Levy, Y. Lipshitz, B. Richter, Z. Shkedi, Y. Wolfson, and K.-H. Speidel, Hyperfine Interact. **5** 283 (1978).
[26]C. Scherer, Nucl. Phys. **A157**, 81 (1970).
[27]M. Blume, Nucl. Phys. **A167**, 81 (1971).
[28]F. Bosch and H. Spehl, Z. Phys. A **268**, 145 (1974); **280**, 329 (1977).
[29]F. Bosch, S. Flaig, and H. Spehl, Z. Phys. A **279**, 141 (1976).
[30]R. Brenn, H. Spehl, A. Weckherlin, H. A. Doubt, and G. Van Middelkoop, Z. Phys. A **281**, 219 (1977).
[31]H. R. Andrews, R. L. Graham, J. S. Geiger, J. R. Beene, O. Häusser, D. Ward, and D. Horn, Hyperfine Interact. **4**, 110 (1978).
[32]G. Seiler-Clark, D. Pelte, H. Emling, A. Balanda, H. Grein, E. Grosse, R. Kulessa, D. Schwalm, H. J. Wollersheim, M. Hass, G. J. Kumbartzki, and K.-H. Speidel, Nucl. Phys. **A399**, 211 (1983).
[33]D. Ward, H. R. Andrews, R. L. Graham, J. S. Geiger, and N. Rud, Nucl. Phys. **A234**, 94 (1974).
[34]H. H. Anderson and J. F. Ziegler, *Hydrogen Stopping Powers and Ranges in All Elements* (Pergamon, New York, 1977).
[35]J. F. Ziegler, *Handbook of Stopping Cross-Sections for Energetic Ions in all Elements* (Pergamon, New York, 1980).
[36]H. Bateman, Proc. Cambridge Philos. Soc. **15**, 423 (1910).
[37]R. D. Evans, *The Atomic Nucleus* (McGraw-Hill, New York, 1955), pp. 490ff.
[38]H. Emling, private communication.
[39]F. James and M. Roos, Comput. Phys. Commun. **10**, 343 (1975).
[40]F. James, Comput. Phys. Commun. **20**, 29 (1980).
[41]F. Rösel, H. M. Fries, K. Alder, and H. C. Pauli, At. Data Nucl. Data Tables **21**, 91 (1978).
[42]B. Bochev, S. A. Karamian, T. Kutsarova, E. Nadjakov, and Yu. Ts. Oganessian, Nucl. Phys. **A267**, 344 (1976).
[43]P. Ring, A. Hayashi, K. Hara, H. Emling, and E. Grosse, Phys. Lett. **110B**, 423 (1982).
[44]F. S. Stephens, Rev. Mod. Phys. **47**, 43 (1975).
[45]G. B. Hagemann, J. D. Garrett, B. Herskind, J. Kowonacki, B. M. Nyakó, P. J. Nolan, and J. F. Sharpey-Schafer, Nucl. Phys. **A424**, 365 (1984).
[46]C. M. Baglin, Nucl. Data Sheets **18**, 223 (1976).
[47]H. J. Wollersheim and Th. W. Elze, Nucl. Phys. **A278**, 87 (1977).
[48]C. M. Baglin, Nucl. Data Sheets **30**, 1 (1980).
[49]B. Harmatz, Nucl. Data Sheets **26**, 281 (1979).
[50]I. Y. Lee, N. R. Johnson, T. T. Sugihara, M. W. Guidry, E. L. Robinson, R. M. Diamond, and F. S. Stephens, ORNL Physics Division Report ORNL-5787, 1981, p. 84.
[51]F. W. N. de Boer, P. Koldewijn, R. Beetz, J. L. Maarleveld, J. Konijn, R. Janssens, and J. Vervier, Nucl. Phys. **A290**, 173 (1977).
[52]R. M. Ronningen, R. B. Piercey, J. H. Hamilton, C. F. Maguire, A. V. Ramayya, H. Kawakami, W. K. Dagenhart, and L. L. Riedinger, Phys. Rev. C **16**, 2218 (1977).
[53]R. M. Diamond, F. S. Stephens, W. H. Kelly, and D. Ward, Phys. Rev. Lett. **22**, 546 (1969).
[54]D. Ward, H. R. Andrews, J. S. Geiger, R. L. Graham, and J. F. Sharpey-Schafer, Phys. Rev. Lett. **30**, 493 (1973).
[55]J. Simpson, P. A. Butler, P. D. Forsyth, J. F. Sharpey-Schafer, J. D. Garrett, G. B. Hagemann, B. Herskind, and L. P. Ekström, J. Phys. G **10**, 383 (1984).
[56]K. Nakai, D. Proetel, R. M. Diamond, and F. S. Stephens, Phys. Rev. Lett. **32**, 1380 (1974).
[57]G. D. Symons and A. C. Douglas, Phys. Lett. **24B**, 11 (1967).
[58]N. Rud, G. T. Ewan, A. Christy, D. Ward, R. L. Graham, and J. S. Geiger, Nucl. Phys. **A191**, 545 (1972).
[59]S. H. Sie, D. Ward, J. S. Geiger, R. L. Graham, and H. R. Andrews, Nucl. Phys. **A291**, 443 (1977).
[60]S. Åberg, Phys. Scr. **25**, 23 (1982).
[61]S. Frauendorf and F. R. May, Phys. Lett. **125B**, 245 (1983).
[62]R. Bengtsson, H. Frisk, F. R. May, and J. A. Pinston, Nucl. Phys. **A415**, 189 (1984).
[63]L. L. Riedinger, S. Frauendorf, H. Ower, L. H. Courtney, M.

P. Fewell, D. R. Haenni, J. S. Hattula, S. A. Hjorth, N. R. Johnson, and I. Y. Lee, in *Proceedings of the Conference on High Angular Momentum Properties of Nuclei,* Oak Ridge, 1982 (Vol. 1—Contributed Papers), edited by N. R. Johnson (Oak Ridge National Laboratory, Oak Ridge, 1982), p. 8.

[64]M. W. Guidry, C.-L. Wu, D. H. Feng, J. N. Ginocchio, X.-G. Chen, and J.-Q. Chen, Phys. Lett. B **176**, 1 (1986).

[65]C.-L. Wu, D. H. Feng, X.-G. Chen, J.-Q. Chen, and M. W. Guidry, Phys. Lett. **168B**, 313 (1986); Phys. Rev. C **36**, 1157 (1987).